**Lifetime, Size and Emission of Laser-Induced Plasmas for In-Situ Analysis on Planetary Bodies.** F. Seel[1], S. Schröder[1], E. Clavé[1], E. Dietz[1], S. Frohmann[1], P. B. Hansen[1], K. Rammelkamp[1], and H.-W. Hübers[1,2] [1]German Aerospace Center (DLR), Institute for Optical Sensor Systems, Berlin, Germany (fabian.seel@dlr.de), [2]Humboldt Universität zu Berlin, Institute of Physics, Berlin, Germany

**Introduction:** When the MSL rover Curiosity landed on Mars in 2012, it successfully demonstrated the use of Laser-Induced Breakdown Spectroscopy (LIBS) for in-situ geochemical investigations of planetary bodies for the first time [1]. Since then, the importance of LIBS for Solar System exploration has only grown, with several subsequent missions employing LIBS systems as part of their sensor suite [2, 3]. With new surface-exploring missions planned for the Moon and Mars, more LIBS instruments may be deployed in the near future. LIBS measurements are performed by focusing a pulsed laser beam on the surface of a sample to generate a local plasma. The emission of this plasma is then analyzed to investigate the sample composition. Since the lifetime, size and emission of the laser-induced plasma depend strongly on experimental parameters [4, 5], LIBS instruments for in-situ analysis of planetary bodies have to be designed for specific environments and science scenarios to generate high-quality data and meet their science goals. Important parameters to consider include the pressure of the atmosphere, the irradiance of the ablating laser and the lithology of the investigated samples.

In this study, we present spatiotemporal measurements of the plasma emission at different atmospheric conditions and laser irradiances for a selection of four samples with different lithologies to aid in the development of new LIBS instruments for in-situ geochemical research of planetary bodies.

**Experimental Setup:** To investigate the lifetime, size and emission of laser-induced plasmas, we use a plasma imaging system that employs a gated ICCD sensor to achieve a temporal resolution of down to 2 ns. The ICCD is most sensitive between about 300 nm and 900 nm. The plasma is generated by a 1064 nm Nd:YAG laser with a pulse duration of 8.1 ns and a spot diameter of about 40 µm.

Different atmospheric conditions can be simulated using a vacuum chamber in which the laser-induced micro plasma is ignited, see Fig. 1. In this study, we focus on atmospheric conditions on Earth, Mars and airless planetary bodies such as the Moon. The Martian environment can be simulated by first evacuating the vacuum chamber and subsequently filling it with Martian analog gas that represents the atmospheric composition on Mars until a pressure of about 700 Pa is reached. Airless bodies are simulated by evacuating the chamber to a pressure of less than 1 Pa.

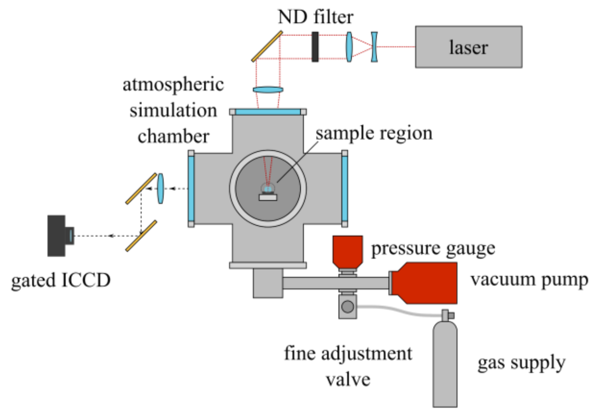


*Figure 1: Overview of the experimental setup. The plasma is induced inside the atmospheric simulation chamber by a laser pulse that can be attenuated using ND filters. A gas supply allows for simulation of Martian atmospheric conditions.*

**Methodology:** For all investigated samples, measurements were performed at terrestrial and Martian atmospheric conditions, as well as in vacuum. The laser pulse energy was varied between 11.86 mJ and 6.56 mJ, which corresponds to average irradiances of about 960 MW/mm² and 560 MW/mm². Four samples with different lithologies were investigated: LMS1 (pressed pellet), LHS1 (pressed pellet), soapstone (talc) and basalt (cut rock). For the purpose of this abstract, we limit the discussion to data from the basalt sample at 8.75 mJ or 710 MW/mm².

Each plasma image is recorded from a single laser shot on a pristine spot on the sample surface to avoid crater formation effects that influence the plasma properties. The data acquisition rate is defined by the laser's pulse frequency of 2 Hz. To account for the varying expansion dynamics and emission of the plasma at different atmospheric conditions and times in the plasma's evolution, the gate time of the ICCD was varied between 2 ns and 200 ns. All images were pre-processed by subtracting a dark image and applying a uniform filter to reduce the noise level. Residual constant offsets were removed by taking the mean value over 100 lines without signal from the plasma emission and subtracting the value from the image.

The total plasma emission was calculated as the sum over each image. To account for the different ICCD gate times, the total emission of each image was normalized with the gate time used for the measurement.

The full width at half maximum sizes $FWHM_{\mathrm{h}}$ of the plasmas were calculated as the largest horizontal

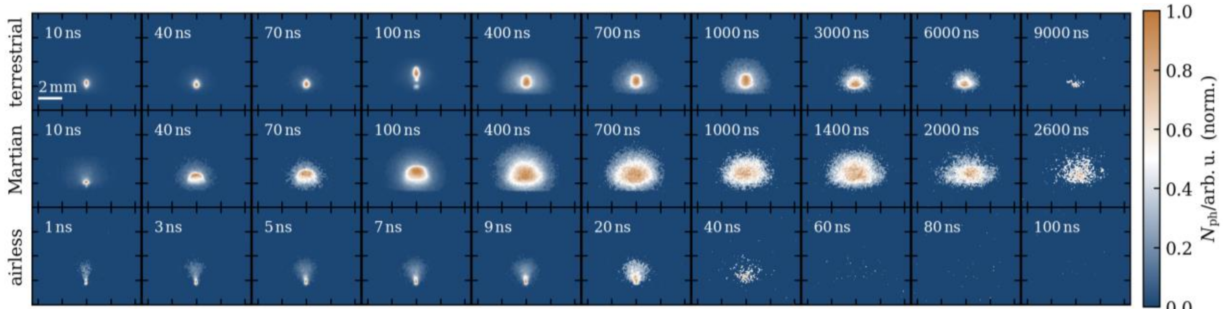


*Figure 2:Time series of plasma images at the three investigated atmospheric conditions. A selection of data is shown. Each plasma image is normalized to its respective maximum signal. Note the different time scales at the three investigated atmospheric conditions.*

distance between points that show half of the maximum plasma emission of a given image.

**Results:** Fig. 2 shows the expansion of the plasma plume from the basalt sample at the three investigated atmospheric conditions for a laser energy of 8.75 mJ. The times after plasma ignition are noted in the top left of each image. All plasma images are normalized to their respective maximum. At 100 ns after plasma ignition, two plasma plumes are visible for the measurement performed at terrestrial conditions. This secondary breakdown is likely initiated on residual ejecta from the previous ablation process.

Overall, a change in the extent of the plasma and its dynamics is visible between different atmospheric conditions. The plasma's lifetime is the longest at terrestrial atmospheric conditions and shortest at airless conditions. At terrestrial conditions, the plasma is most confined, with a maximum horizontal extent of about

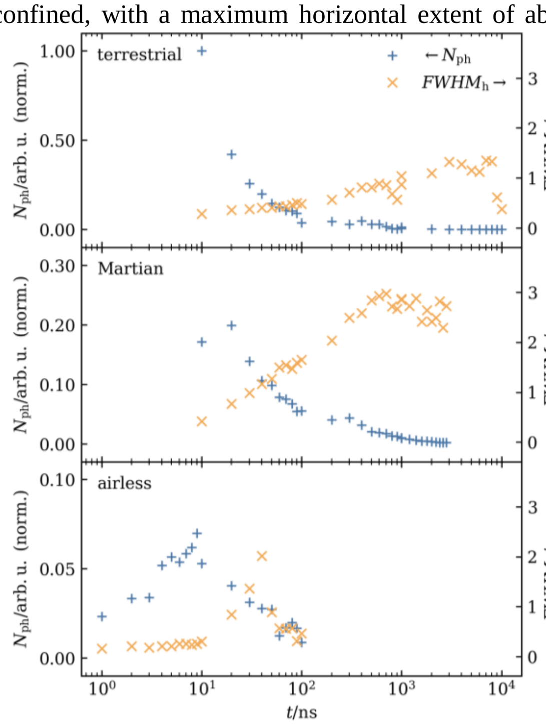


*Figure 3: Comparison of the development of the total emitted plasma radiation and the plasma's horizontal $FWHM_h$ for the three investigated atmospheric conditions. Note the different scales of the y-axes.*

1.5 mm. While the plasma remains confined at Martian atmospheric conditions, it is larger with a maximum horizontal extent of about 3 mm. At airless conditions, the plasma extends freely into the vacuum, which leads to a small and bright plasma core close to the sample surface. The uninhibited expansion results in a maximum horizontal extent of about 2 mm.

In Fig. 3, the total emission of the plasma is compared for the three different atmospheric conditions, again with a laser energy of 8.75 mJ. For easier comparison, the data is normalized to the strongest emission at terrestrial conditions. On the secondary y-axis, the $FWHM_h$ is plotted for comparison. At terrestrial atmospheric conditions, the plasma is brightest at 10 ns after plasma ignition. The plasma reaches its maximum horizontal extend of about 1.5 mm around 3 µs after ignition. For Martian conditions, the peak emission occurs after about 20 ns and is about 20% of the peak emission at terrestrial conditions. The plasma reaches its maximum extend of about 3 mm around 500 ns after ignition. This is close to the field of view of Mars 2020's SuperCam instrument at 4 m [2]. Finally, for airless conditions the peak plasma emission is reduced to about 7% of the peak emission at terrestrial conditions. The plasma reaches its maximum extent of about 2 mm around 40 ns after ignition.

**Conclusion:** The presented data show the different behaviors of plasmas ignited at different atmospheric conditions. The maximum extent varies between about 1.5 mm for terrestrial conditions, 3 mm for Martian conditions and 2 mm for airless conditions. The plasma is brightest at Terrestrial atmospheric conditions. At Martian and airless conditions, the plasma's peak emission is about 20% and 7% of that at terrestrial conditions, respectively.

**References:** [1] Maurice, S. et al. (2016) *J. Anal. At. Spectrom., 31(4)*, 863-889. [2] Maurice, S. et al. (2021) *Space Sci. Rev., 217*, 1-108. [3] Wan, X. (2021) *At. Spectrosc., 42(6)*, 294-298. [4] Singh, J. P. and Thakur, S. N. (Eds.). (2020). Laser-induced breakdown spectroscopy. Elsevier. [5] Lasue, J. et al. (2012) *J. Geophys. Res. Planets, 117*, (E1).